Improved Wong and classical approximations, and reduction of fusion data

L. F. Canto,[1,*] V. A. B. Zagatto,[2,†] J. Lubian,[2,‡] and R. Donangelo[3,§]

[1]*Instituto de Física, Universidade Federal do Rio de Janeiro, CP 68528, 21941-972, Rio de Janeiro, RJ, Brazil*

[2]*Instituto de Física, Universidade Federal Fluminense, Av. Litoranea s/n, Gragoatá, Niterói, R.J., 24210-340, Brazil*

[3]*Instituto de Física, Facultad de Ingeniería, Universidad de la República, Av. Julio Herrera y Reissig 565, 11300 Montevideo, Uruguay*

(Received 18 December 2023; revised 12 March 2024; accepted 24 April 2024; published 9 May 2024)

We present an improved version of the Wong formula for heavy-ion fusion, where the parameters of the parabolic approximation of the Coulomb barrier are replaced by parameters of the l-dependent potential at an effective partial wave. A pocket formula for this l dependence is given. This version reproduces the fusion cross sections of quantum-mechanical calculations very well, even when the original Wong formula is invalid. The same procedure is used to derive an improved expression for the classical fusion cross section, which is very accurate at above-barrier energies. Based on this classical expression, we propose a new method to reduce fusion data in this energy range. This method is used to perform a comparative study of complete fusion suppression in collisions of weakly bound projectiles. This study indicates that the suppression of complete fusion is essentially due to the action of nuclear breakup couplings.

DOI: 10.1103/PhysRevC.109.054609

I. INTRODUCTION

The dynamics of fusion reactions are highly complex, especially in collisions of projectiles with low breakup thresholds (lower than 3 or 4 MeV) [1–6]. Owing to the low binding energy, the projectile can break up as it approaches the target, giving rise to different fusion processes. First, is the direct complete fusion (DCF), where the whole projectile fuses with the target. This is the usual fusion reaction, observed also in the collisions of tightly bound nuclei. In addition, the breakup of the projectile triggers two more fusion processes: the incomplete fusion (ICF) and the sequential complete fusion (SCF). The former occurs when at least one, but not all, projectile fragments fuse with the target. The latter takes place when all breakup fragments fuse sequentially with the target. Experimentally, SCF cannot be distinguished from DCF. The experimental cross section corresponds to complete fusion (CF), the sum DCF + SCF. Besides, many experiments cannot distinguish CF from ICF. Then, the data correspond to total fusion (TF), the sum of all fusion processes.

In collisions of weakly bound projectiles, the low breakup threshold affects the CF cross section in two ways. Owing to the low binding energy, the projectile's density has a long tail, leading to a reduction of the Coulomb barrier. This is a static effect, which enhances CF at all collision energies. On the other hand, the low breakup threshold leads to strong breakup couplings, diverting an appreciable part of the incident flux into the breakup channel. This is a dynamic effect that hinders CF. In this way, the CF data is the net result of the competition between the opposing static and dynamic effects of the low binding energy of the projectile. Experimental and theoretical studies indicate that the CF cross section is enhanced at subbarrier energies and suppressed above the Coulomb barrier [1–6]. However, the present understanding of CF reactions is not entirely satisfactory. New experimental and theoretical studies are called for.

There are different methods to assess the influence of the low breakup threshold of the projectile on the CF cross section. The first is to compare the CF data to predictions of theoretical models that do not consider the projectile's low binding. A standard procedure is to compare them to fusion cross sections of one-channel calculations with a standard real potential and short-range absorption. Usually, one adopts implementations of the double-folding model with standard nuclear densities, like the São Paulo (SPP) [7,8] or the Akyüz-Winther (AW) [9] potential. A more straightforward approach is to compare the data to predictions of semiclassical or classical approximations to the quantum-mechanical (QM) treatment, like the barrier penetration model (BPM), the Wong formula [10], or even the classical fusion cross section. However, one should ensure that the approximate model for the theoretical cross section is valid under the conditions of the experiment. Then, the differences between the experimental and the theoretical cross sections are assumed to arrive from the low binding energy of the projectile.

The other possibility is to compare CF data of the weakly bound system to fusion data of similar tightly bound systems. However, direct comparisons of the data would be meaningless since they are strongly dependent on the charges and masses of the collision partners. Thus, submitting the data to some reduction procedure that eliminates the influence of such trivial factors is necessary. Several reduction procedures have

*canto@if.ufrj.br
†vzagatto@id.uff.br
‡jlubian@id.uff.br
§donangel@fing.edu.uy

been proposed (for a review, see Ref. [11]). A very efficient one is the fusion function (FF) reduction method, which is based on the Wong formula [10]. In an ideal situation where the fusion cross section is unaffected by the collision partners' intrinsic structure, and the Wong formula approximates the QM cross section, the reduced data is well described by a universal fusion function. Then, this universal function is used as a benchmark to assess the importance of channel coupling effects in the fusion data. However, the Wong formula is not a good approximation to the QM cross section for light systems at subbarrier energies and at energies well above the barrier [12–14].

In the present paper, we discuss the limitations of the Wong formula and the classical expression for the fusion cross section. We show that their validity can be extended if one replaces the s-wave barrier parameters with effective barrier parameters obtained by proper angular-momentum averages. Then, we propose a new reduction method for the above-barrier fusion data based on this improved version of the classical cross section. This method is used to study CF data of weakly bound systems.

The paper is organized as follows: In Sec. II, we discuss the use of complex interactions in potential scattering to simulate the effects of fusion and total reaction in the scattering wave function. In Sec. III, we introduce the classical and Wong approximations to the QM fusion cross section. We then discuss the validity of these approximations and the classical limit of the Wong formula. In Sec. IV, we develop new versions of Wong and the classical approximations and then propose a new reduction method based on the latter. In Sec. V, we use the new reduction method to perform a comparative study of CF data in collisions of ^{6}Li, ^{7}Li, ^{9}Be, and ^{6}He on several targets. Finally, in Sec. VI, we give the main conclusions of the present paper.

II. THE FUSION AND THE REACTION CROSS SECTIONS IN POTENTIAL SCATTERING

In an idealized situation where the intrinsic degrees of freedom of the collision partners do not affect the collision, the elastic cross section can be described by potential scattering. In this approach, the colliding nuclei are treated as point particles, interacting through Coulomb and nuclear forces. The scattering wave function is expanded in partial waves and the resulting radial wave functions are calculated by solving the radial equation with the l-dependent potential

$$V_l(r) = V_{\rm N}(r) + V_{\rm C}(r) + \frac{\hbar^2 l(l+1)}{2\mu r^2}. \tag{1}$$

Above, $V_{\rm N}(r)$ is the nuclear interaction between the projectile and the target, where r is the distance between them. It can be obtained by integrating the densities multiplied by a properly chosen nucleon-nucleon interaction (folding model). The São Paulo (SPP) [7,8] and the Akyüz-Winther (AW) [9] potentials are implementations of the folding model, using different approximations. They are widely used in the literature.

The Coulomb potential is usually approximated as

$$V_{\rm C}(r) = \frac{Z_{\rm P}Z_{\rm T}e^2}{2R_{\rm C}}\left(3 - \frac{r^2}{R_{\rm C}^2}\right) \text{ for } r < R_{\rm C}$$
$$= \frac{Z_{\rm P}Z_{\rm T}e^2}{r} \text{ for } r \geqslant R_{\rm C}. \tag{2}$$

Above, $R_{\rm C}$ is the Coulomb radius, corresponding to the sum of the radii of the collision partners, and $Z_{\rm P}$ and $Z_{\rm T}$ are the atomic numbers of the projectile and the target, respectively.

The third term in Eq. (1) is the centrifugal potential, which accounts for the tangential kinetic energy in the radial equation. It is inversely proportional to the reduced mass, μ, and grows quadratically with the angular momentum ($\sim l^2$ for large l).

The attractive nuclear potential is very strong but has a short range. On the other hand, the repulsive Coulomb and centrifugal terms are weaker but have longer ranges. The competition between the attractive and repulsive terms leads to a barrier in the potential $V_l(r)$, located at R_l and with height B_l.

However, actual nucleus-nucleus collisions are always affected by intrinsic degrees of freedom, which are coupled with the coordinate r. Then, a fraction of the incident flux is diverted into nonelastic channels along the collision. In potential scattering, this effect is simulated by the addition of an attractive imaginary part to the nuclear potential, namely,

$$V_{\rm N}(r) \longrightarrow U_{\rm N}(r) = V_{\rm N}(r) + iW(r).$$

In this way, the S-matrix loses its unitarity, giving rise to an absorption cross section. For a collision with energy E (wave number k), it is given by

$$\sigma_{\rm abs}(E) = \frac{\pi}{k^2}\sum (2l+1)P_{\rm abs}(l,E). \tag{3}$$

Above, $P_{\rm abs}(l,E)$ is the absorption probability,

$$P_{\rm abs}(l,E) = 1 - |S_l(E)|^2, \tag{4}$$

where $S_l(E)$ is the lth component of the S matrix.

The characteristics of the imaginary potential depend on the nuclear reactions whose effects it is simulating. This point is discussed below.

A. The total reaction cross section

The elastic cross section is influenced by fusion and nonelastic processes. The former only takes place when the densities of the collision partners overlap strongly. On the other hand, the latter are dominant in grazing collisions, where the distance of closest approach is larger than the barrier radius. Then, if one wants to evaluate the total reaction cross section, which has contributions of both reaction mechanisms, the imaginary potential must be very strong in the inner region of the barrier but also act in the neighborhood of the barrier radius. Then, the range of $W(r)$ must be similar to that of the real part of the nuclear potential.

Frequently, the imaginary potential used in calculations of the total reaction cross section is represented by a

Woods-Saxon (WS) function,

$$W_{\rm R}(r) = -\frac{W_0}{1+\exp\left[(r-R_{\rm w})/a_{\rm w}\right]}. \tag{5}$$

Above,

$$R_{\rm w} = r_{\rm w}\left(A_{\rm P}^{1/3} + A_{\rm T}^{1/3}\right), \tag{6}$$

where $A_{\rm P}$ and $A_{\rm T}$ stand respectively for the mass numbers of the projectile and the target. Adopting parameters of the order $W_0 \simeq 50$ MeV, $r_{\rm w} \approx 1.2$ fm, and $a_{\rm w} \approx 0.6$ fm, the imaginary potential has the desired behavior.

Another possibility is to take the imaginary potential proportional to the real one. That is, one writes

$$U_{\rm N}(r) = (1+\beta i)V_{\rm N}(r), \tag{7}$$

where β is a constant, usually close to one. Gasques *et al.* [15] used the SPP together with imaginary potentials of this kind to successfully analyze experimental scattering and total reaction data of a large number of systems.

B. The fusion cross section

An imaginary potential to simulate the effects of fusion in potential scattering must lead to total absorption in the inner region of the barrier and be negligible elsewhere. This behavior is guaranteed by a WS function like that of Eq. (5) with a short range, i.e., with parameters like

$$W_0 \simeq 50\ {\rm MeV},\ r_{\rm w} \approx 1.0\ {\rm fm},\ {\rm and}\ a_{\rm w} \approx 0.2\ {\rm fm}. \tag{8}$$

Denoting by $S_l^{\rm F}(E)$ and $P_{\rm F}(l,E)$ the partial-wave components of the S matrix and the corresponding fusion probability in a calculation with the imaginary potential of Eqs. (5) and (8), the fusion cross section can be written as

$$\sigma_{\rm F}(E) = \frac{\pi}{k^2}\sum_{l=0}^{\infty}(2l+1)P_{\rm F}(l,E), \tag{9}$$

with

$$P_{\rm F}(l,E) = 1 - \left|S_l^{\rm F}(E)\right|^2. \tag{10}$$

We remark that similar results can be obtained with a real nuclear potential but adopting ingoing wave boundary conditions [16]. This approach is used in the CCFULL computer code [17], frequently used in coupled-channel calculations.

The above discussion suggests that the fusion probability in Eq. (9) is equivalent to the probability of the incident wave reaching the strong absorption region. In this way, the fusion cross section could be approximated by the cross section of the barrier penetration model (BPM),

$$\sigma_{\rm BPM}(E) = \frac{\pi}{k^2}\sum_{l=0}^{\infty}(2l+1)aaT(l,E). \tag{11}$$

Above, $T(l,E)$ is the transmission coefficient for the system to go through the barrier of the potential $V_l(r)$ in a collision with energy E. It is calculated by Kemble's version [18] of the Wenzel-Kramers-Brillouin (WKB) approximation, through the expression

$$T(l,E) \equiv T_{\rm WKB}(l,E) = \frac{1}{1+\exp\left[2\Phi(l,E)\right]}. \tag{12}$$

TABLE I. Barrier parameters of the São Paulo potential for the systems discussed in the text. The barrier radii are expressed in fm and height and curvature parameters are given in MeV.

System	$R_{\rm B}$	$V_{\rm B}$	$\hbar\omega$
^{7}Li + ^{27}Al	8.5	6.1	2.4
^{7}Li + ^{209}Bi	11.4	29.4	4.1
^{24}Mg + ^{138}Ba	11.1	81.6	3.9

At subbarrier energies, $\Phi(l,E)$ is the integral of the imaginary wave number between the classical turning points. That is,

$$\Phi(l,E) = \int_{r_i}^{r_e}\kappa_l(r)dr, \tag{13}$$

where

$$\kappa_l(r) = \sqrt{\frac{2\mu}{\hbar^2}[V_l(r)-E]}. \tag{14}$$

The internal (r_i) and external (r_e) turning points are determined by the conditions

$$V_l(r_i) = E,\ r_i < R_l \text{ and } V_l(r_e) = E,\ r_e \geqslant R_l. \tag{15}$$

However, this prescription cannot be used above the barrier, with no real turning points. A solution to this problem was found by Hill and Wheeler [19]. First, they approximated the potential barrier by the parabola

$$V(r) \simeq B_l - \tfrac{1}{2}\mu\omega_l^2(r-R_l)^2, \tag{16}$$

where B_l, R_l, and $\hbar\omega_l$ are the height, radius, and barrier curvature parameters. Of particular interest are the parameters for the Coulomb barrier, denoted by

$$V_{\rm B} \equiv B_{l=0},\ R_{\rm B} \equiv R_{l=0},\ \text{and}\ \hbar\omega \equiv \hbar\omega_{l=0}. \tag{17}$$

Next, they carried out the analytical continuation of the collision coordinate onto the complex plane and found the complex turning points (see also Ref. [20]). In this way, the WKB integral of Eq. (13) could be evaluated analytically, and they found the result

$$\Phi(l,E) = \frac{\pi}{\hbar\omega}(B_l - E). \tag{18}$$

We compared BPM cross sections to those obtained by solving the one-channel radial equations with a short-range imaginary potential. These cross sections are denoted by $\sigma_{\rm BPM}$ and $\sigma_{\rm F}^{\rm 1ch}$, respectively. We also compared the total reaction cross sections, denoted by $\sigma_{\rm R}^{\rm 1ch}$.

We considered a light, ^{7}Li + ^{27}Al, an intermediate, ^{7}Li + ^{209}Bi, and a heavy system, ^{24}Mg + ^{138}Ba. Here, and throughout the present work, we adopt the SPP for the real part of the nuclear potential. The barrier parameters of the parabolic expansion of $V_{l=0}(r)$ for the above-mentioned systems are listed in Table I. In the calculations of $\sigma_{\rm F}^{\rm 1ch}$, we used strong absorption imaginary potentials with a short range. They were given by a WS function with the parameters of Eq. (8). In the calculations of $\sigma_{\rm R}^{\rm 1ch}$, the imaginary potential was given by Eq. (7), with $\beta = 0.78$ [15].

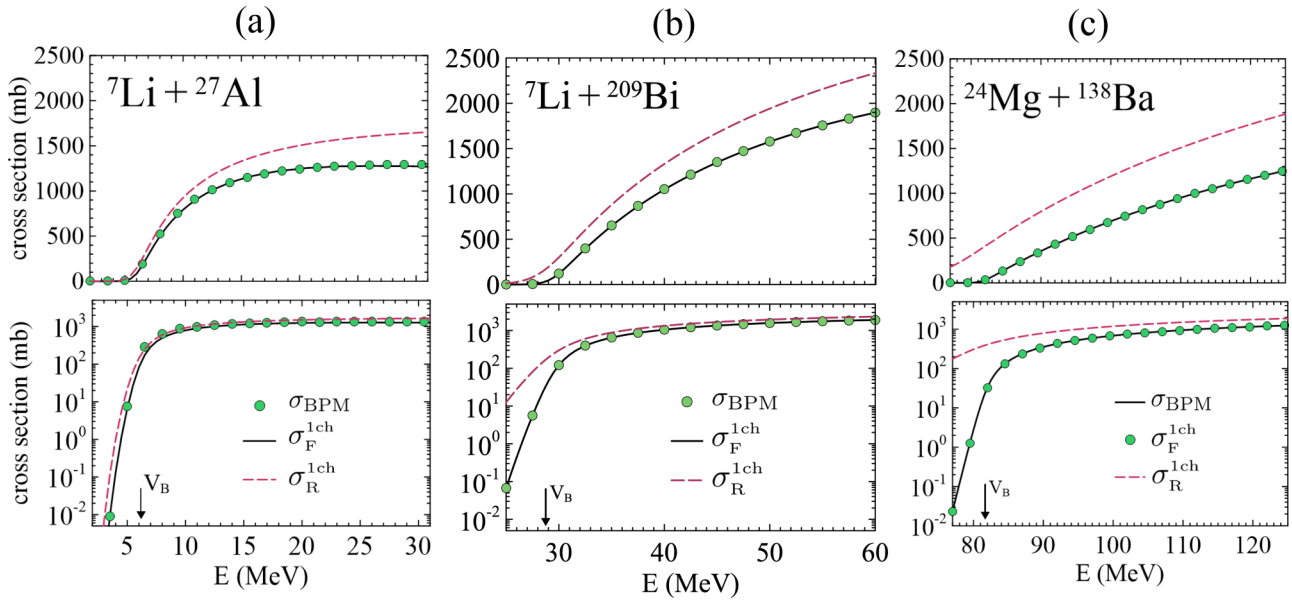

FIG. 1. Comparison of BPM fusion cross sections, σ_{BPM}, with fusion cross sections of QM calculations with the SPP and short-range absorption, σ_F^{1ch}, for three systems in different mass regions. For comparison, we also show cross sections of QM calculations with the long-range imaginary potential of Eq. (7), σ_R^{1ch}.

The σ_{BPM}, the σ_F^{1ch}, and the σ_R^{1ch} cross sections for the ^{7}Li + ^{27}Al, ^{7}Li + ^{209}Bi, and ^{24}Mg + ^{138}Ba systems are shown in Fig. 1. The calculations were performed at collision energies ranging from ≈4 MeV below V_B to ≈30 MeV above it. In each case, the results are presented in linear and logarithmic scales, appropriate for comparisons at the above-barrier and subbarrier energies, respectively. We find that the σ_F^{BPM} and the σ_F^{1ch} cross sections for the three systems are really very close. The corresponding curves can hardly be distinguished in the figures. On the other hand, the total reaction cross sections are much larger than the other two, mainly at subbarrier energies. This is not surprising since σ_R^{1ch} has contributions from absorption beyond the barrier radius, which remains relevant even at collision energies well below V_B. Then, we stress that the BPM is a very good approximation to fusion but very different from the total reaction cross section.

Since σ_{BPM} is practically identical to the QM fusion cross section, σ_F^{1ch}, we henceforth consider the former as the benchmark cross section to assess the accuracy of approximate expressions.

III. THE CLASSICAL AND THE WONG APPROXIMATIONS TO THE FUSION CROSS SECTION

A. The classical approximation

At high enough collision energies (the meaning of high enough will be clarified later), one can use the classical approximation for the fusion cross section. To derive it, one makes the following assumptions:

(1) The sum of partial waves involves many l values, so that the angular momentum can be treated as a continuous variable λ:

$$l \to \lambda = l + 1/2. \tag{19}$$

In this way, the sum over partial-waves becomes an integral, namely,

$$\sum_{l=0}^{\infty}(2l+1) \to \int_{\lambda=1/2}^{\infty} 2\lambda d\lambda. \tag{20}$$

Then, one replaces in Eq. (1): $l(l+1) = \lambda^2 - 1/4$, and one gets the λ-dependent potential

$$V_\lambda(r) = V_N(r) + V_C(r) + \frac{\hbar^2}{2\mu r^2}(\lambda^2 - 1/4). \tag{21}$$

(2) Next, one neglects the λ dependence of R_λ and $\hbar\omega_\lambda$, and writes

$$R_\lambda = R_B, \quad \hbar\omega_\lambda = \hbar\omega. \tag{22}$$

In this way, one gets the barrier heights

$$B_\lambda = V_B + \frac{\hbar^2}{2\mu R_B^2}(\lambda^2 - 1/4). \tag{23}$$

(3) Tunneling effects are neglected, so that the transmission coefficient becomes

$$T(\lambda, E) \simeq T_{cl}(\lambda, E) = 1 \text{ for } \lambda \leqslant \lambda_g$$
$$= 0 \text{ for } \lambda > \lambda_g. \tag{24}$$

Above, λ_g is the grazing angular momentum in a collision with energy E, given by the condition

$$B_{\lambda_g} = E. \tag{25}$$

Using the explicit form of B_λ, within the approximation of Eq. (23), one gets the relation

$$\lambda_g^2 - \frac{1}{4} = \frac{2\mu R_B^2}{\hbar^2}(E - V_B). \tag{26}$$

Within the above approximations, we can derive an analytical expression for the fusion cross section of Eq. (11). One gets

$$\sigma_{cl}(E) = \frac{\pi}{k^2}\int_{\lambda=1/2}^{\infty} 2\lambda T(\lambda, E)d\lambda, \tag{27}$$

or, using Eq. (24),

$$\sigma_{cl}(E) = \frac{\pi}{k^2}\int_{\lambda=1/2}^{\lambda_g} 2\lambda d\lambda = \frac{\pi}{k^2}\left(\lambda_g^2 - \frac{1}{4}\right). \tag{28}$$

Then, using Eq. (26), one gets the classical fusion cross section

$$\begin{aligned}\sigma_{cl}(E) &= \pi R_B^2\left(1 - \frac{V_B}{E}\right) \text{ for } E \geqslant V_B \\ &= 0 \text{ for } E < V_B.\end{aligned} \tag{29}$$

The classical fusion cross section has a serious flaw: it vanishes at subbarrier energies.

B. The Wong formula

Wong [10] derived an analytic expression for the fusion cross section which includes tunneling effects. To get his formula, Wong made the same assumptions as in the derivation of the classical cross section, except for the transmission coefficient of Eq. (24). Instead, he used the Hill-Wheeler transmission coefficient,

$$T_{HW}(l, E) = \frac{1}{1 + \exp\left[\frac{2\pi}{\hbar\omega}(V_B - E)\right]}, \tag{30}$$

below and above the barrier. Then, Eq. (27) becomes

$$\sigma_W(E) = \frac{\pi}{k^2}\int_{\lambda=1/2}^{\infty} \frac{2\lambda d\lambda}{1 + \exp\left[\frac{2\pi}{\hbar\omega}(V_B - E)\right]}. \tag{31}$$

The above integral can be evaluated analytically; the result is the Wong formula,

$$\sigma_W = \frac{\hbar\omega R_B^2}{2E}\ \ln\left\{1 + \exp\left[\frac{2\pi}{\hbar\omega}(E - V_B)\right]\right\}. \tag{32}$$

For future purposes, we write the above equation in the form

$$\sigma_W = \sigma_0 F_0(x), \tag{33}$$

where

$$\sigma_0 = \frac{\hbar\omega R_B^2}{2E} \tag{34}$$

is a characteristic (energy-dependent) strength of the cross section, and

$$F_0(x) = \ln[1 + e^{2\pi x}] \tag{35}$$

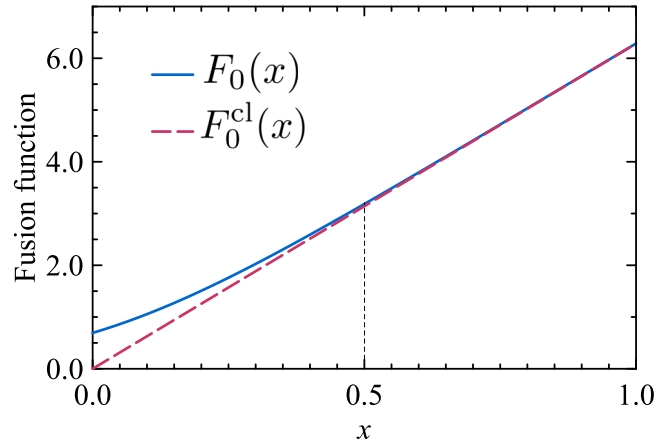

FIG. 2. The Wong fusion function and its asymptotic limit.

is the universal fusion function (UFF) [12,13], which is expressed in terms of the dimensionless energy variable

$$x = \frac{E - V_B}{\hbar\omega}. \tag{36}$$

1. The classical limit of the Wong formula

For $2\pi x \gg 1$, one can approximate: $1 + \exp(2\pi x) \simeq \exp(2\pi x)$ and one gets the classical limit of the universal fusion function

$$F_0^{cl}(x) = 2\pi x. \tag{37}$$

The convergence of $F_0(x)$ to its classical limit is illustrated in Fig. 2. Comparing the two curves, one concludes that the universal fusion function can be safely approximated by Eq. (37) for $x \gtrsim 0.5$. Since typical values of $\hbar\omega$ are between 2 and 4 MeV, the classical cross section of Eq. (29) is very close to σ_W, starting at ≈1.5 MeV above V_B. Then, at energies above this limit, we can insert the classical limit of the Wong fusion function into Eq. (35) and get the classical fusion cross section of Eq. (29), namely,

$$\sigma_W^{cl}(E) = \pi R_B^2\left(1 - \frac{V_B}{E}\right) \text{ for } E \geqslant V_B.$$

2. Validity of the Wong formula

The Wong formula is a very nice analytical expression, but its validity is limited. It is a very good approximation to the QM fusion cross section in collisions of heavy systems ($Z_P Z_T > 500$) at near-barrier energies [13]. However, it is not appropriate for light systems or at collision energies well below or well above the barrier.

The accuracy of the Wong formula is illustrated in Fig. 3, which shows comparisons between σ_W and σ_{BPM} for the ^{7}Li + ^{27}Al ($Z_P Z_T = 39$), ^{7}Li + ^{209}Bi ($Z_P Z_T = 249$), and ^{24}Mg + ^{138}Ba ($Z_P Z_T = 672$) systems. As in the previous figures, the results are shown at collision energies ranging from 4 MeV below the Coulomb barrier to 30 MeV above it. Comparing the cross sections for the ^{7}Li + ^{27}Al system at subbarrier energies, one concludes that the Wong formula overestimates σ_{BPM} drastically. At $E = 2$ MeV (≈4 MeV below V_B), the Wong cross section is wrong by more than one order of

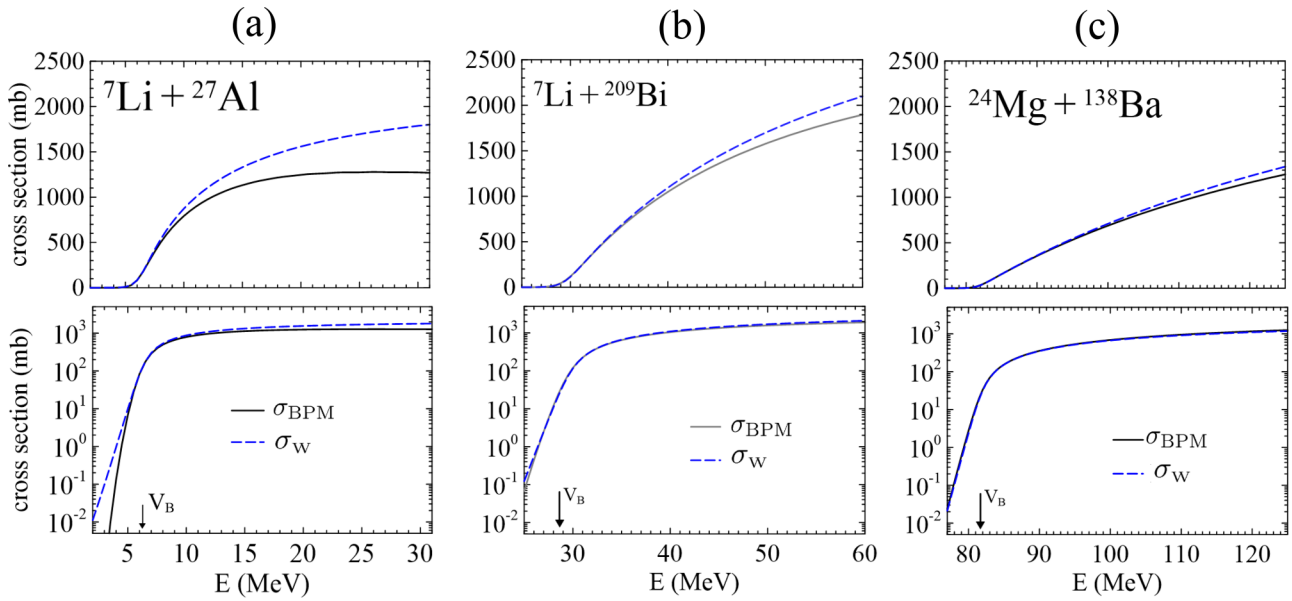

FIG. 3. The Wong fusion cross section in comparison with the cross sections predicted by the BPM. See the text for details.

magnitude. For the two heavier systems, the Wong formula is quite close to σ_{BPM} in this energy region. At above-barrier energies, σ_W is systematically larger than σ_{BPM}, mainly in the case of the ^{7}Li + ^{27}Al. At 30 MeV above V_B, the Wong cross section for this system overestimates σ_{BPM} by ≈45%. The situation is better for the other two heavier systems. For the ^{7}Li + ^{209}Bi and ^{24}Mg + ^{138}Ba systems at the same energy above V_B, σ_W exceeds σ_{BPM} by 10% and ≈5%, respectively. The exceedingly large values of the Wong cross section above the Coulomb barrier can be traced back to neglecting the angular-momentum dependence of the barrier parameters. A detailed discussion of the failure of the Wong formula is presented below.

At subbarrier energies, the cross section results exclusively from tunneling effects. Thus, it is susceptible to the shape of the potential barrier. Figure 4 shows the Coulomb barriers and the parabolic fits for the three systems of Fig. 3. The potential axes are truncated at the lowest collision energies of our calculations, namely, $V(r) = V_B - 4$ MeV. The comparison between the potential barrier of the ^{7}Li + ^{27}Al system and the parabolic fit sheds light on the abnormally large values of the Wong cross section at subbarrier energies. The parabolic barrier is much thinner than the actual Coulomb barrier. Thus, the transmission coefficient for the parabola is unrealistically large. This leads to a considerable enhancement of σ_W in comparison to σ_{BPM}. Conversely, the parabolic fits for the barriers of the two heavier systems are quite reasonable. Besides, the fitted barrier is thicker on the inner side of the barrier but thinner on the outer side. Then, there is some compensation in calculating the transmission factors, and the Wong formula reproduces the QM cross sections well.

Now, we consider the Wong formula above the Coulomb barrier. In this case, the differences between σ_W and σ_{BPM} arise from the neglect of the angular-momentum dependencies of R_λ and $\hbar\omega_\lambda$. However, we have shown that the Wong cross section reduces to the classical cross section just above the Coulomb barrier, and this cross section does not depend on the barrier curvature. Then, we concentrate on the angular-momentum dependence of R_λ. Table II shows the explicit value of the highest energy considered in our calculations for each system, namely, $E_{max} = V_B + 30$ MeV. The next two columns show the corresponding values of the grazing angular momentum and the barrier radius associated with it. They are represented by λ_g and R_g, respectively. The table also shows the s-wave barrier radius and the ratio R_g^2/R_B^2. This ratio estimates the inaccuracy of Wong and the classical expressions in the worst scenario of the present calculations.

In the ^{7}Li + ^{27}Al collision at $E = 36$ MeV, the angular-momentum dependence of R_λ is significant. If one uses R_g^2 instead of R_B^2 in the Wong or the classical expression, as proposed by Rowley and Hagino [21], the cross section is reduced by a factor of ≈2. The situation is better for the ^{7}Li + ^{209}Bi and mainly the ^{24}Mg + ^{138}Ba systems, where the reduction factors would be considerably closer to one (0.83 and 0.91, respectively).

TABLE II. Variation of the barrier radii as the angular momentum varies from zero to its grazing value for the systems discussed in the text. Column two gives the maximal energy considered in our calculations. For each system, it corresponds to the Coulomb barrier plus 30 MeV. The remaining columns are explained in the text. The grazing angular momenta are given in $\hbar$ units; the barrier radii are given in fm.

System	E_{max} (MeV)	λ_g	R_g	R_B	R_g^2/R_B^2
^{7}Li + ^{27}Al	36	20	6.2	8.5	0.53
^{7}Li + ^{209}Bi	60	34	10.4	11.4	0.83
^{24}Mg + ^{138}Ba	112	59	10.6	11.1	0.91

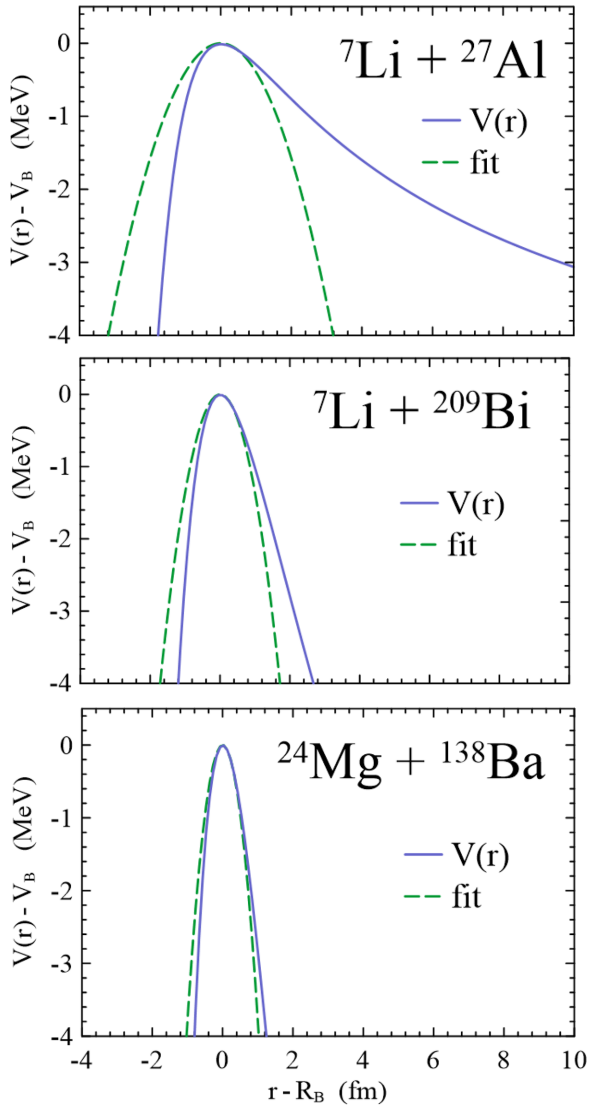

FIG. 4. The Coulomb barriers for the ^{7}Li + ^{27}Al, ^{7}Bi + ^{209}Al, and ^{24}Mg + ^{138}Ba systems, in comparison with the corresponding parabolic fits.

IV. IMPROVED VERSIONS OF THE WONG AND THE CLASSICAL CROSS SECTIONS

Two papers reported improvements in the original Wong formula (32). One was already mentioned at the end of the previous section [21]. The other was another paper by Wong [22]. Wong reported corrections to the original formula due to the continuum approximation of the discrete angular momentum l. Besides, he proposed a method to improve the description of the fusion cross section by determining the experimental barrier for each angular momentum from the low-energy fusion cross section. In this way, the modified Wong formula can describe the fusion data better than the barrier penetration model devised in the original approximation, considering the influence of particular nuclear structure effects on the fusion cross section. Although it is a nice feature of this formula, it is unsuitable for the reduction of fusion data, which is the main concern of the present work. The fusion function reduction method, which will be discussed in Sec. IV B, requires that the Wong formula be a good description of the BPM cross section rather than the data.

To reduce fusion data, one seeks a *bare* potential to provide a so-called nominal Coulomb barrier. This potential should lead to good descriptions of experimental cross sections of systems where particular nuclear structure properties have no significant influence on fusion. A good candidate is the potential of the double-folding model, evaluated systematically by an integral of the matter densities of the colliding nuclei with a realistic nucleon-nucleon interaction. The São Paulo potential [7,8] implements this model based on realistic matter densities given by a two-parameter Fermi distribution. Another good candidate is the Akyüz-Winther [9] potential, given by a Woods-Saxon approximation to the double folding potential. The parameters of the WS function are obtained through a systematic study involving many systems distributed over a broad mass range. The SPP and the AW potentials provide similar fusion cross sections, as reported in Ref. [23].

In this section and throughout the present paper, we adopt the São Paulo potential. This potential has been widely used in studies of weakly bound systems, including systematic investigations of reduced fusion cross sections [13], the energy dependence of the optical potential, seeking the so-called breakup threshold anomaly [24], and theoretical predictions of CF and ICF cross sections in collisions of weakly bound stable and neutron halo radioactive projectiles [25–27]. It has also been used as the *bare* potential in many coupled reaction channels calculations of multinucleon transfer reactions together with elastic, inelastic, and charge-exchange angular distributions (see, for example, Refs. [28–30]).

The previous subsection showed that the Wong formula works poorly for light systems at energies well below or above the Coulomb barrier. The problem can be fixed by introducing effective barrier parameters, $\overline{R}$ and $\hbar\bar{\omega}$, in the modified Wong formula,

$$\overline{\sigma}_{\rm W} = \frac{\hbar\bar{\omega}\overline{R}^2}{2E}\,\ln\left\{1+\exp\left[\frac{2\pi}{\hbar\bar{\omega}}(E-V_{\rm B})\right]\right\}. \qquad (38)$$

Since the behavior of the cross section at subbarrier energies is determined by the argument of the exponential, $2\pi(E-V_{\rm B})/\hbar\bar{\omega}$, we keep the original values of the barrier parameters in the slowly varying multiplicative factor. That is, we approximate

$$\frac{\hbar\bar{\omega}\overline{R}^2}{2E} \simeq \frac{\hbar\omega R_{\rm B}^2}{2E}. \qquad (39)$$

Then, we get the effective barrier curvature parameter, $\hbar\bar{w}$, by imposing that the modified Wong cross section of Eq. (38) be equal to the fusion cross section of the barrier penetration model. We find

$$\hbar\bar{\omega} = 2\pi(E-V_{\rm B})\Big/\ln\left[\exp\left(\frac{2E\sigma_{\rm BPM}}{\hbar\omega R_{\rm B}^2}-1\right)\right]. \qquad (40)$$

At above-barrier energies, the main contributions to the fusion cross section come from angular momenta in the vicinity of $\lambda_{\rm g}$. This led Rowley and Hagino [21] to propose an improved version of the Wong formula. It consists of replacing

R_B and $\hbar\omega$ with barrier parameters for λ_g. The Wong formula then becomes

$$\sigma_W^g = \frac{\hbar\omega_g R_g^2}{2E} \ln\left\{1+\exp\left[\frac{2\pi}{\hbar\omega_g}(E-V_B)\right]\right\}, \quad (41)$$

where we used the short-hand notation $\hbar\omega_g \equiv \hbar\omega_{l_g}$.

As can be seen in Table II, the barrier radius decreases as λ increases, and replacing R_B^2 with R_g^2 in the Wong formula reduces the cross section at above-barrier energies. Since the Wong formula overestimates σ_{BPM} (see Fig. 3), this modification is expected to improve the agreement between the two cross sections. However, it might overestimate the weight of the grazing angular momentum in the partial-wave series. This possibility is avoided in the improved Wong cross section proposed below.

Since the system Hamiltonian depends on λ quadratically (through the centrifugal term of the potential), we assume that the angular-momentum dependence of the barrier radius is also quadratic, at least around $\lambda = 0$. Then, we make a series expansion of R_λ and keep only the term of lowest order. We get

$$R_\lambda \simeq R_B - \gamma\lambda^2, \quad (42)$$

where γ is a system-dependent parameter.

Then, we define the effective barrier radius in a collision with energy E and grazing angular momentum λ_g as the weighted average,

$$\overline{R} = \langle R_\lambda\rangle_\lambda = \frac{1}{N}\int_0^{\lambda_g} 2\lambda d\lambda [R_B - \gamma\lambda^2], \quad (43)$$

where N is the norm

$$N = \int_0^{\lambda_g} 2\lambda d\lambda. \quad (44)$$

At above-barrier energies, the integrations involve large values of λ. Then, it is a reasonable approximation to use $\lambda = 0$ (instead of $\lambda = 1/2$) as the lower limit of the integrations in Eqs. (43) and (44). Following this procedure, we get

$$\overline{R} = R_B - \gamma\frac{\lambda_g^2}{2}. \quad (45)$$

Comparing the above expression with Eq. (42), one concludes that $\overline{R}$ corresponds to the barrier radius of the λ-dependent potential of Eq. (21) at the effective angular momentum

$$\lambda_{rms} = \sqrt{\langle\lambda^2\rangle_\lambda} = \frac{\lambda_g}{\sqrt{2}}. \quad (46)$$

Thus, we can write

$$\overline{R} = R_{\lambda_{rms}}. \quad (47)$$

Note that $\overline{R}$ is fully determined by Eqs. (47) and (46). Therefore, one does not need the explicit value of the coefficient γ in the expansion of Eq. (42).

The curvature parameter can be modified in the same way, namely,

$$\hbar\overline{\omega} = \langle\hbar\omega_\lambda\rangle_\lambda = \hbar\omega_{\lambda_{rms}}. \quad (48)$$

The improved Wong cross section at above-barrier energies is then given by Eq. (38), with the $\overline{R}$ and $\hbar\overline{\omega}$ parameters of the above equations.

An improved version of the classical cross section of Eq. (29) can be derived by the same procedure. Replacing R_B with $\overline{R}$, one gets

$$\overline{\sigma}_{cl} = \pi\overline{R}^2\left(1-\frac{V_B}{E}\right) \text{ for } E \geqslant V_B$$
$$= 0 \text{ for } E < V_B. \quad (49)$$

It is convenient to introduce the dimensionless energy variable,

$$y = 1 - \frac{V_B}{E}. \quad (50)$$

Then, the standard classical cross section takes the form

$$\sigma_{cl} = \pi R_B^2 y, \quad (51)$$

and its improved version can be written as

$$\overline{\sigma}_{cl} = f_R(y)\sigma_{cl}. \quad (52)$$

Above, $f_R(y)$ is the correction factor

$$f_R(y) = \left[\frac{\overline{R}(y)}{R_B}\right]^2, \quad (53)$$

which is always less than one. To stress the energy-dependence (or y-dependence) of $\overline{R}$, we used the notation $\overline{R}(y)$. One may notice that the $\overline{R}(y)$ value may be obtained directly from the $f_R(y)$ function. The next section will present an empirically obtained version of this function.

Figure 5 shows the approximate cross sections σ_W^g [Eq. (41)], $\overline{\sigma}_W$ [Eq. (38)] and $\overline{\sigma}_{cl}$ [Eq. (52)], for the ^{7}Li + ^{27}Al, ^{7}Li + ^{209}Bi, and ^{24}Mg + ^{138}Ba systems. They are represented by dashed lines, blue circles, and red stars, respectively. The solid lines correspond to the BPM cross sections. First, one notices that σ_W^g (dashed lines) actually underestimates σ_{BPM} at above-barrier energies. The difference between the two cross sections is particularly large in the case of the light ^{7}Li + ^{27}Al system. The difference is smaller for the ^{7}Li + ^{209}Bi system, and the agreement is very good for ^{24}Mg + ^{138}Ba. On the other hand, the improved Wong fusion cross sections ($\overline{\sigma}_W$) for the three systems are in excellent agreement with the corresponding σ_{BPM} below and above the Coulomb barrier. One also observes that, at above-barrier energies, the improved classical cross sections, $\overline{\sigma}_{cl}$, reproduce σ_{BPM} equally well, except in a very small energy interval just above V_B.

A. An approximate expression for $\overline{R}$

The barrier parameters of the real potential, V_B, R_B, and $\hbar\omega$, can be obtained from available computer codes. However, the effective barrier radius, $\overline{R}$, is more complicated to obtain, as it is necessary to determine the function $f_R(y)$, of Eq. (53). We carried out a systematic study of this function, considering several systems over a broad mass range, and two commonly used nuclear interactions: the SPP [7,8] and the AW [9,31] potentials. In each case, we evaluated $f_R(y)$ for collision energies ranging from $E = V_B$ to $E = 2\times V_B$. The results for

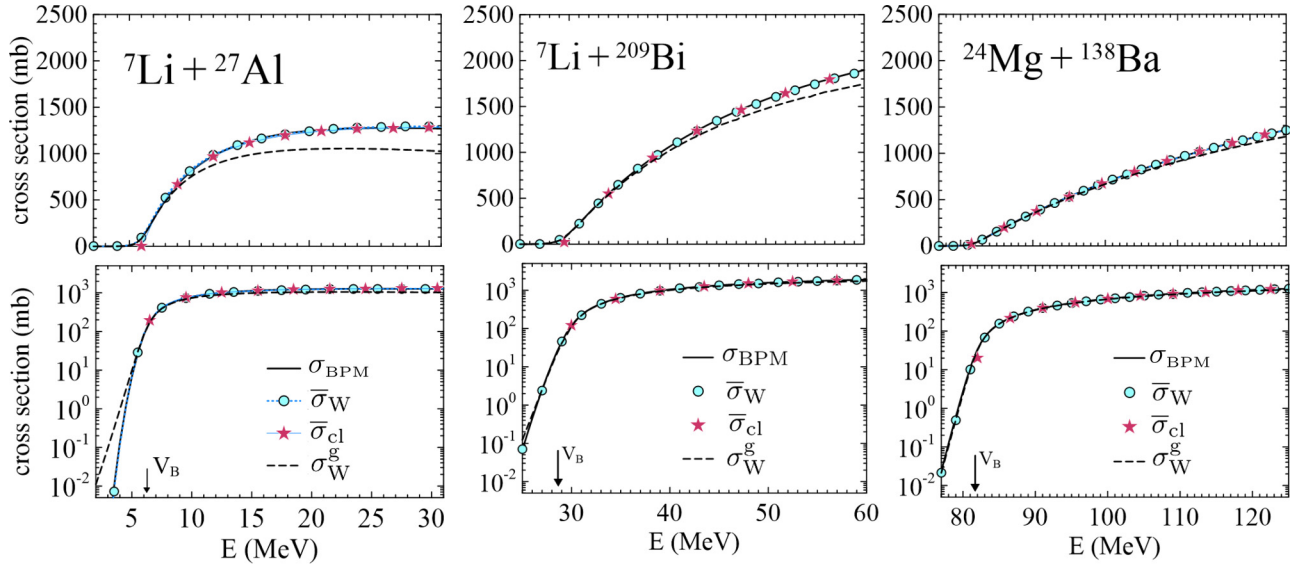

FIG. 5. The BPM fusion cross sections for the ^{7}Li + ^{27}Al, ^{7}Li + ^{209}Bi, and ^{24}Mg + ^{138}Ba systems, in comparison to those obtained by the improved versions of the Wong formula, σ^{g}_{W} and $\overline{\sigma}_{W}$. The improved classical cross sections, $\overline{\sigma}_{cl}$, are also shown.

the SPP and for the AW interactions are shown in Figs. 6(a) and 6(b), respectively. The points correspond to the effective barrier radius numerically calculated at a mesh of collision energies.

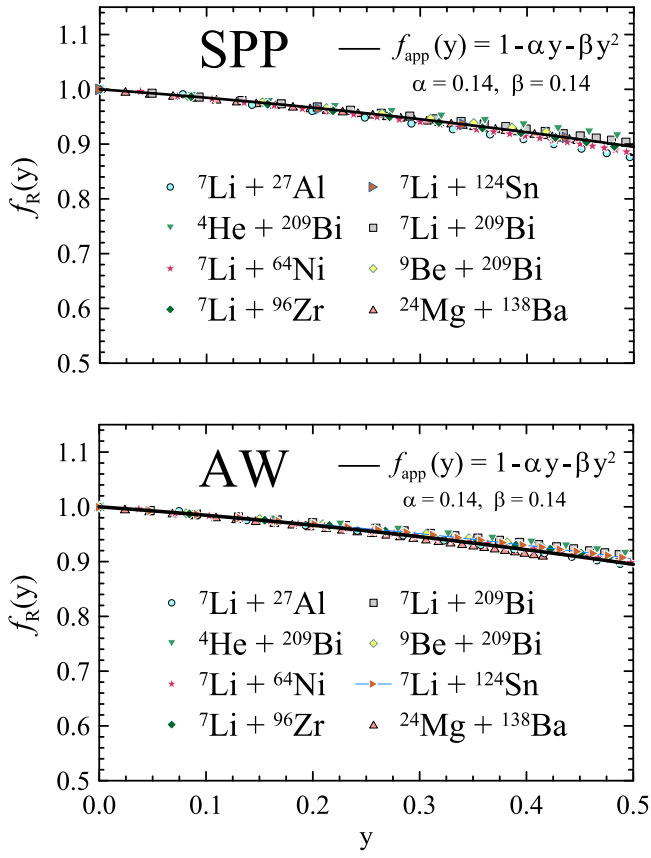

FIG. 6. The function $f_R(y)$ of Eq. (53), for the ^{7}Li + ^{27}Al, ^{7}Li + ^{209}Bi, and ^{24}Mg + ^{138}Ba systems, plotted versus the dimensionless energy variable, y.

The solid line represents the pocket formula

$$f_{app}(y) = 1 - 0.14y - 0.14y^2, \tag{54}$$

which gives the best fit to the data. Inspecting Figs. 6(a) and 6(b), one concludes that $f_R(y)$ has a very weak dependence on the system. For all systems, $f_R(y)$ is given by Eq. (54) as an excellent approximation. Furthermore, one notices that this conclusion is valid for both the SPP and the AW potentials. Then, the dependence of $\overline{\sigma}_W$ and $\overline{\sigma}_{cl}$ on the nuclear potential occurs exclusively through the S-wave barrier parameters.

The improved version of the Wong formula presented in this section is valid for any choice of nuclear potential. The only requirement is that R_B, V_B, and $\hbar\omega$ be the parameters of the parabolic approximation of the barrier in the BPM calculation. On the other hand, the validity of the pocket formula has been demonstrated exclusively for the SPP and the AW potentials. However, we should keep in mind that the angular-momentum dependence of R_λ and $\hbar\omega_\lambda$ arises exclusively from the centrifugal term of the total potential in the radial equation. For this reason, we believe that the pocket formula remains valid for any choice of nuclear interaction.

B. Reduction of fusion data and universal functions

A frequently used reduction procedure is the fusion function (FF) method [12,13], which is based on the Wong formula. The collision energy E and the fusion cross section σ_F are transformed into the dimensionless quantities

$$E \to x = \frac{E - V_B}{\hbar\omega}, \quad \sigma_F \to F(x) = \frac{\sigma_F}{\sigma_0}, \tag{55}$$

where σ_0 is the characteristic cross section of Eq. (34).

The improved Wong cross section of Eq. (38) leads to an improved fusion function (IFF) method, implemented by the transformations

$$E \to \overline{x} = \frac{E - V_B}{\hbar\overline{\omega}}, \quad \sigma_F \to \overline{F}(\overline{x}) = \frac{\sigma_F}{\overline{\sigma}_0}. \tag{56}$$

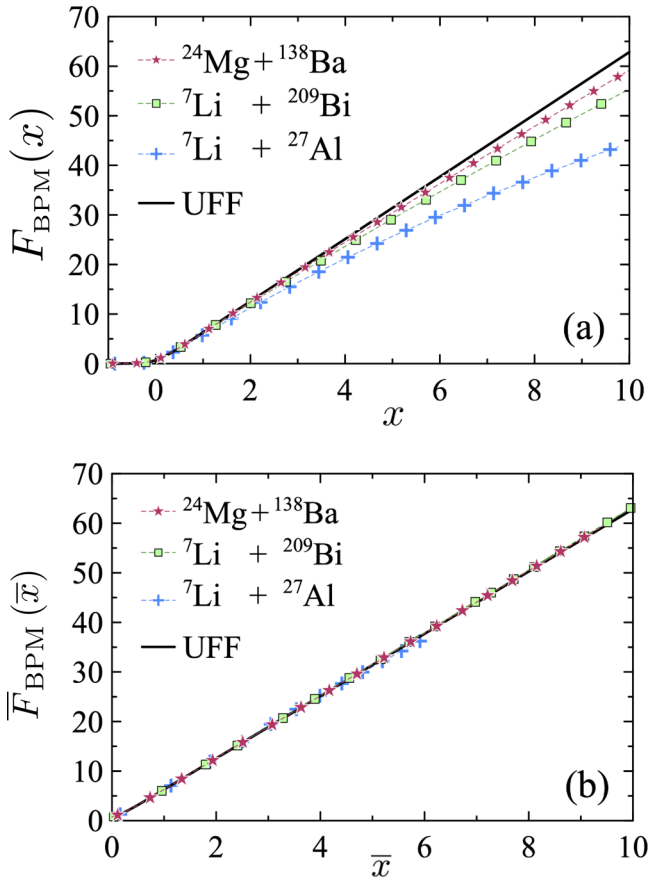

FIG. 7. Reduced BPM cross sections for the ^{7}Li + ^{27}Al, ^{7}Li + ^{209}Bi, and ^{24}Mg + ^{138}Ba systems, reduced by the two fusion function procedures discussed in the text.

Above, $\hbar\bar{\omega}$ is the effective barrier curvature parameter of Eq. (40), and $\overline{\sigma}_0$ is the characteristic cross section of the improved Wong formula,

$$\overline{\sigma}_0 = \frac{\hbar\bar{\omega}\overline{R}^2}{2E}. \tag{57}$$

As a simple test, the reduction procedures can be applied to the BPM fusion cross section [11,13]. The procedure is successful if reduced cross sections for systems in different mass ranges are very similar. Furthermore, if the procedure leads to a universal function, the reduced cross sections should be very close to it. We applied this test to the two versions of the fusion function method, Eqs. (55) and (56).

Figure 7(a) shows the reduced $\sigma_{\rm BPM}$ fusion cross sections for the ^{7}Li + ^{27}Al, ^{7}Bi + ^{209}Al, and ^{24}Mg + ^{138}Ba systems. They are denoted by $F_{\rm BPM}(x)$. The reduction was carried out through the standard fusion function method of Eq. (55). For comparison, the UFF is also shown (black solid line). One notices that the fusion functions exhibit a significant system dependence. At the highest energies, corresponding to $x \approx 10$ ($\approx$25 MeV above $V_{\rm B}$), the fusion function for the ^{7}Li + ^{27}Al system is $\approx$30% lower than the UFF. The fusion functions for the two heavier systems remain below the UFF, but the difference is much smaller. Despite this system dependence, the fusion method has been widely used in comparing fusion data of weakly bound systems [13,32–37]. In practical studies of nuclear structure effects based on this reduction method, the fusion functions are renormalized to avoid system dependencies arising from the inaccuracy of the Wong formula [13].

Next, we apply the same test to the improved fusion function method of Eq. (56). The reduced cross sections, shown in Fig. 7(b), are denoted by $\overline{F}_{\rm BPM}(\overline{x})$. Now, the situation is entirely different. The system dependence of the previous figure is fully eliminated. The fusion functions for different systems can hardly be distinguished, and they agree very well with the UFF.

The fact that the improved classical cross section of Eq. (49) is very close to $\sigma_{\rm BPM}$ leads to another universal function, which we denote by $G_0(y)$. It is obtained by the transformations

$$E \to y = 1 - \frac{V_{\rm B}}{E}, \quad \overline{\sigma}_{\rm cl} \to G_0 = \frac{\overline{\sigma}_{\rm cl}}{\pi\overline{R}^2}. \tag{58}$$

In this way, one gets the *classical fusion line* (CFL)

$$G_0(y) = y. \tag{59}$$

The above transformation suggests a new reduction procedure to analyze fusion data at energies above the Coulomb barrier. The energy is transformed into the dimensionless energy variable, y, as in Eq. (58), and the fusion cross section, $\sigma_{\rm F}$, is transformed into the *classical fusion function* (CFF),

$$\overline{G}(y) = \frac{\sigma_{\rm F}}{\pi\overline{R}^2} = \frac{\sigma_{\rm F}}{\pi R_{\rm B}^2 f_{\rm R}(y)}. \tag{60}$$

Above, $f_{\rm R}(y)$ is the ratio $\overline{R}^2/R_{\rm B}^2$, introduced in Eq. (53). We submitted the classical fusion function (CFF) reduction method of Eqs. (58) and (60) to the same test applied to the fusion function method. Since the empirical function $f_{\rm app}(y)$ is quite close to $f_{\rm R}(y)$, we used the approximate expression

$$\overline{G}^{\rm expt}(y) = \frac{\sigma_{\rm F}^{\rm expt}}{\pi f_{\rm app}(y) R_{\rm B}^2}. \tag{61}$$

The reduced $\sigma_{\rm BPM}$ cross sections, denoted by $\overline{G}_{\rm BPM}(y)$, for the ^{7}Li + ^{27}Al, ^{7}Bi + ^{209}Bi, and ^{24}Mg + ^{138}Ba systems are shown in Fig. 8. The black solid line represents the classical fusion line of Eq. (59). We observe that the reduced cross sections for the three systems are extremely close and agree very well with the classical fusion line.

An interesting point in Fig. 8 is that the results for heavier systems are concentrated at the lower region of the CFL, whereas those for lighter systems reach the high end of this line. The reason is that our calculations were performed at energies up to $\approx V_{\rm B} + 30$ MeV. In this way, the largest y value in the calculations is

$$y_{\rm max} = 1 - \frac{V_{\rm B}}{V_{\rm B} + 30\ {\rm MeV}}.$$

Then, for the lightest systems, ^{7}Li + ^{27}Al, the barrier ($V_{\rm B} = 6.1$ MeV) is much lower than 30 MeV and $y_{\rm max}$ is close to one. For the heaviest system, ^{24}Mg + ^{138}Ba, the barrier ($V_{\rm B} = 81, 6$ MeV) is much larger than 30 MeV, so that $y_{\rm max}$ is much lower.

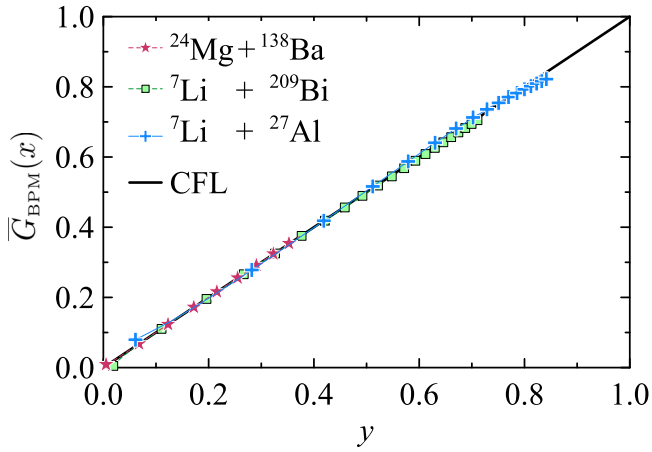

FIG. 8. Reduced BPM cross sections for the same systems as the previous figure, but the CFF method now carries out the reductions.

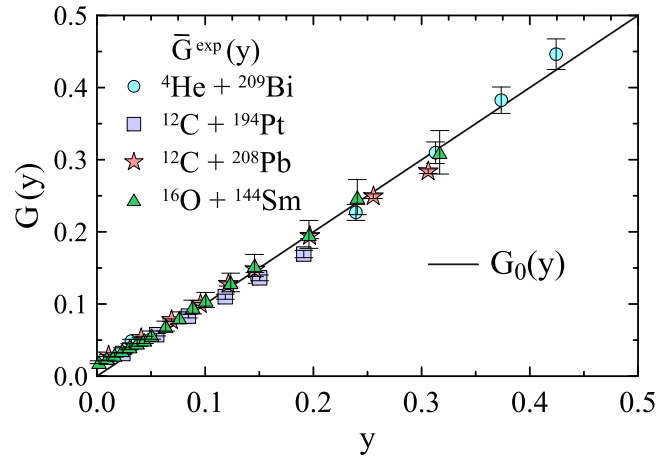

FIG. 9. Experimental CFF for a few tightly bound systems with negligible channel coupling effects.

Note that, above the Coulomb barrier, the fusion cross section does not depend on the barrier curvature. This can be seen explicitly in the expression for $\overline{\sigma}_{\rm cl}$but needs to be clarified in the Wong formula. However, it becomes transparent if one uses the classical limit of $F_0(x)$ [Eq. (37)]. Then, the dependence on $\hbar\omega$ cancels when $F_0(x)$ is multiplied by σ_0.

V. APPLICATION: REDUCED CROSS SECTIONS OF WEAKLY BOUND SYSTEMS

The experimental fusion functions evaluated by the IFF method are very similar to those reduced by the standard FF method, reported in Ref. [12]. The advantage of the former over the latter method is that it does not require a renormalization to take care of the inaccuracies of the Wong formula. However, the results of the two methods are very similar. For this reason, the discussion of the present section will be focused on the CFF reduction method.

We used the CFF method to reduce the fusion data of several tightly and weakly bound systems, performing the transformations

$$E \longrightarrow y = 1 - \frac{V_{\rm B}}{E}, \quad \overline{G}^{\rm expt}(y) = \frac{\sigma_{\rm F}^{\rm expt}}{\pi \overline{R}^2}. \tag{62}$$

To accomplish this goal, one needs the barrier height of the potential, $V_{\rm B}$, and the effective barrier radius $\overline{R}$.

A. Comparative study of experimental CFFs

In this section, we apply the CFF reduction method to the fusion data of weakly bound systems.

Before considering weakly bound systems, we submitted the CFF method to a test similar to the one carried out in Sec. IV B. The difference is that instead of applying it to BPM cross sections, we reduce experimental fusion cross sections of tightly bound systems where nuclear structure properties do not influence the cross section at above-barrier energies. In such cases, one expects the reduced fusion data to be very close to the classical fusion line of Eq. (59).

Figure 9 shows the experimental CFF for the ^{4}He + ^{209}Bi [38], ^{12}C + ^{194}Pt [39], ^{12}C + ^{208}Pb [40], and ^{16}O + ^{144}Sm [41] systems. To obtain the CFFs in this section, we use Eq. (62), with $\pi\overline{R}^2 = \pi f_{\rm app}(y) R_{\rm B}^2$, where $R_{\rm B}$ was derived using the São Paulo potential with realistic nuclear densities and $f_{\rm app}(y)$ by the pocket formula of Eq. (54). The values of $V_{\rm B}$ are given in Table III. One observes that the reduced data points are, indeed, very close to the classical fusion line.

Now, we study CFFs associated with the CF of weakly bound projectiles. As we show below, the reduced data of these systems can be fitted by a linear function through the origin of the form

$$\overline{G}^{\rm expt}(y) = \alpha y. \tag{63}$$

TABLE III. Barrier parameters of the SPP for the systems studied in Figs. 9 and 10.

System	$R_{\rm B}$ (fm)	$V_{\rm B}$ (MeV)	$\hbar\omega$ (MeV)
^{4}He + ^{209}Bi	10.6	21.3	4.7
^{12}C + ^{194}Pt	11.3	55.6	4.1
^{12}C + ^{208}Pb	11.5	57.7	4.1
^{16}O + ^{144}Sm	10.8	61.4	3.9
^{6}Li + ^{90}Zr	9.6	16.6	3.4
^{6}Li + ^{124}Sn	10.3	19.5	3.6
^{6}Li + ^{197}Au	11.1	28.7	4.1
^{6}Li + ^{198}Pt	11.1	28.3	4.1
^{6}Li + ^{209}Bi	11.2	29.8	4.2
^{7}Li + ^{124}Sn	10.4	19.3	3.3
^{7}Li + ^{197}Au	11.3	28.3	3.8
^{7}Li + ^{198}Pt	11.3	27.9	3.7
^{7}Li + ^{209}Bi	11.4	29.4	3.8
^{9}Be + ^{208}Pb	11.5	38.5	3.9
^{6}He + ^{209}Bi	11.6	16.4	3.4
^{6}He + ^{238}U	11.9	21.0	3.4

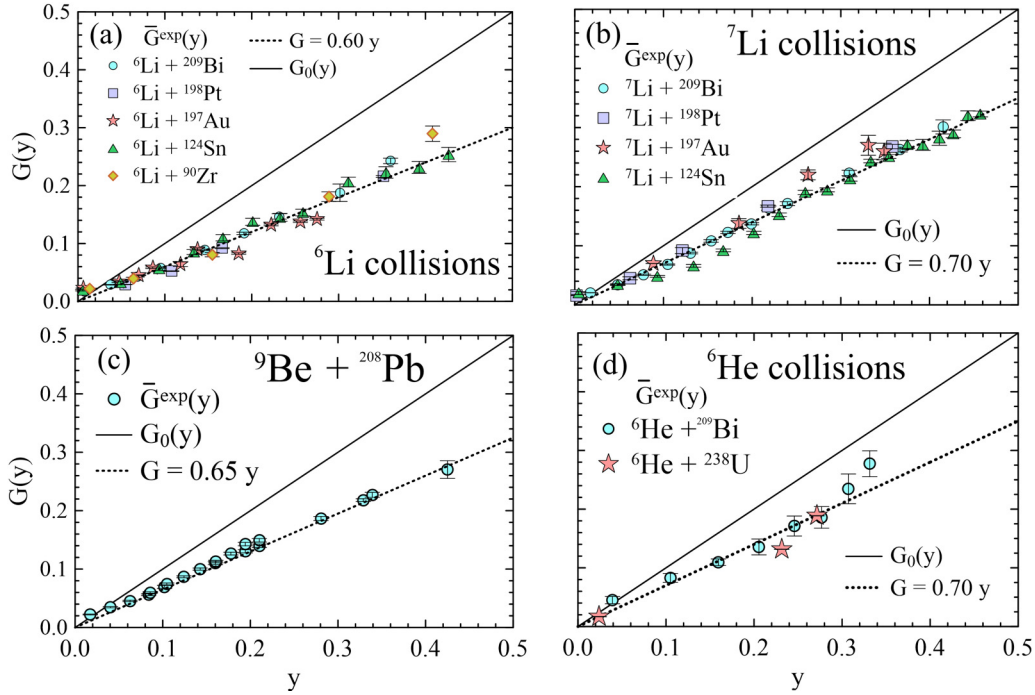

FIG. 10. Experimental CFF for weakly bound projectiles with different targets: (a) collisions of ^{6}Li, (b) collisions of ^{7}Li, (c) collisions of ^{9}Be, (d) collisions of ^{6}He. See the text for details.

Since the classical fusion line is given by this function with $\alpha = 1$, the angular coefficient for a weakly bound projectile can be interpreted as a CF survival factor. This probability is usually called the *suppression factor*. We do not adopt this terminology here, because it is not intuitive: a large suppression factor corresponds, actually, to a small suppression, and the other way around. Figure 10 shows experimental CFFs for several weakly bound systems. In Fig. 10(a), the projectile is ^{6}Li, which has a breakup threshold of 1.47 MeV, and the targets are ^{209}Bi, ^{198}Pt, ^{197}Au, ^{124}Sn, and ^{90}. The data are from Refs. [42,43] (^{6}Li + ^{209}Bi), [44] (^{6}Li + ^{198}Pt), [45] (^{6}Li + ^{197}Au), [46] (^{6}Li + ^{124}Sn), and [47] (^{6}Li + ^{90}Zr). Note that we are considering targets over a significant mass range. The atomic and mass numbers of the targets are comprised of the intervals {40, 83} and {124, 209}, respectively. One finds that the experimental CFF of these systems are very similar. They follow closely the linear function of Eq. (63), with the CF survival factor

$$\alpha^{^6\mathrm{Li}} = 0.60. \tag{64}$$

Next, we consider collisions of ^{7}Li projectiles, which have a breakup threshold of 2.47 MeV. Figure 10(b) shows the CFFs corresponding to the fusion data for the ^{209}Bi [42,43], ^{198}Pt [48], ^{197}Au [45,49], and ^{124}Sn [46] targets. Qualitatively, the figure is very similar to the previous one. The experimental CFF points for these targets are also distributed along a straight line but with a slightly larger CF survival factor

$$\alpha^{^7\mathrm{Li}} = 0.70. \tag{65}$$

Comparing Figs. 10(a) and 10(b), one observes that the CF survival factor decreases with the breakup threshold of the projectile, as expected. However, these figures reveal another very interesting behavior of the CF suppression: it seems independent of the target charge. The results for ^{90}Zr ($Z_T = 40$) are essentially the same as those for the ^{209}Bi target ($Z_T = 83$), which has an atomic number about twice as large. Note that the same conclusion was reached in the study of Kumawat *et al.* [47]. This finding suggests that the Coulomb breakup does not affect the CF cross section. Thus, one is led to the conclusion that the observed CF suppression in collisions of weakly bound projectiles with heavy targets is due to nuclear breakup. This conclusion seems to contradict our knowledge of breakup reactions, which are strongly influenced by Coulomb breakup and Coulomb-nuclear interference [50–53].

However, there is a significant difference between the breakup and the fusion processes. The former gets contributions from hundreds of partial waves, most corresponding to distant collisions, where the distance of closest approach is larger than the range of the nuclear potential. At lower partial waves, nuclear couplings are also relevant, and there are strong Coulomb-nuclear interference effects. Nuclear couplings dominate only at the lowest partial waves. However, their contributions are small due to the factor $(2l + 1)$ contained in the partial-wave expansion of the breakup cross section.

The fusion process is quite different. At high angular momenta, the centrifugal barrier prevents the system from reaching the strong absorption region, where the fusion processes occur. Thus, it is unsurprising that Coulomb couplings play a major role in the breakup process, but they have a negligible influence on the CF cross section. Then, only $l \lesssim l_g$ contributes to fusion, and the nuclear couplings are dominant at these angular momenta.

Now we discuss the collisions of ^{9}Be projectiles. They are also very interesting since their breakup threshold is only 1.65 MeV. There are available CF data for collisions of ^{9}Be with several targets: ^{144}Sm [54], ^{197}Au [35,55,56], ^{186}W [57], and ^{208}Pb [43]. A comparative study of the CF data of these systems, reduced by the fusion function method, was presented in Fig. 13 of Ref. [35]. This comparison was inconclusive since the data did not show any trend. The CF survival factors for systems in the same mass range differed considerably. However, we emphasize that the data for different targets were measured by different groups using different experimental techniques. Thus, a detailed study of the experimental procedures of each experiment would be needed before one can draw reliable conclusions and this would be beyond the scope of the present work. Nevertheless, the data for the $^{9}\mathrm{Be}+{}^{208}\mathrm{Pb}$ and the $^{6,7}\mathrm{Li}+{}^{209}\mathrm{Bi}$ systems, analyzed in the previous two figures, were measured by the same group using similar experimental techniques. Then, we restrict our study to $^{9}\mathrm{Be}+{}^{208}\mathrm{Pb}$.

The experimental CFF for the $^{9}\mathrm{Be}+{}^{208}\mathrm{Pb}$ system is shown in Fig. 10(c), compared with the classical fusion line. One finds that the reduced data points are also distributed along the linear function of Eq. (63), but now the CF survival factor is

$$\alpha^{^{9}\mathrm{Be}} = 0.65. \tag{66}$$

Note that ita value is intermediate between $\alpha^{^{6}\mathrm{Li}}$ and $\alpha^{^{7}\mathrm{Li}}$. Since the breakup threshold of this nucleus lies between those of the two Li isotopes, this result is consistent with the assumption that the CF survival factor decreases with the breakup threshold of the projectile.

Finally, we look at collisions of the two-neutron halo nucleus ^{6}He. Since experiments involving unstable beams are much more challenging, fusion data involving ^{6}He projectiles are very scarce. Nevertheless, there are good CF data for the $^{6}\mathrm{He}+{}^{209}\mathrm{Bi}$ system at several collision energies and the $^{6}\mathrm{He}+{}^{238}\mathrm{U}$ system at a few collision energies. In typical situations, CF followed by the evaporation of two neutrons, cannot be distinguished from ICF events with the capture of the ^{4}He cluster. However, the CF cross sections could be measured under special conditions of these experiments. Kolata *et al.* [58,59] measured the CF cross section for the $^{6}\mathrm{Li}+{}^{209}\mathrm{Bi}$ system at near-barrier energies. The CF of this system leads to the formation of the ^{215}At, which evaporates 1, 2, 3, and 4 neutrons. The cross section was determined by measuring the characteristic alpha particles emitted by the ^{212}At and ^{211}At residual nuclei, which, according to statistical model code predictions [58,59], are the dominant decay modes within the energy interval of the experiment. The ^{212}At and ^{211}At are also formed by the breakup of the projectile, followed by the capture of the ^{4}He cluster (ICFα). However, owing to excitation energy considerations [27], these nuclei could not emit the alpha particles detected in the experiment. Nevertheless, they are expected to make a small contribution to the data points at the highest collision energies.

The CF cross section for the $^{6}\mathrm{He}+{}^{238}\mathrm{U}$ system was measured by Raabe *et al.* [60]. In this case, the signature of CF events was the detection of two fission fragments emitted back to back, unaccompanied by a third charged fragment with a projectile-like kinematic. In fact, the same residual nucleus can be formed by the CF and the ICFα processes after the evaporation of different numbers of neutrons (two more neutrons in the case of CF). However, comparing the fission barrier with the excitation energies in the CF and ICFα processes, one concludes that the latter does not contribute to the measured cross section [27].

Figure 10(d) shows the experimental CFFs corresponding to the CF data of the $^{6}\mathrm{He}+{}^{209}\mathrm{Bi}$ and $^{6}\mathrm{He}+{}^{238}\mathrm{U}$ systems. One observes that the results exhibit the same behavior as the CFFs for ^{7}Li projectiles. The data points of both systems are very close to the black dotted line, which corresponds to the function of Eq. (65). Note that the experimental CFF tends to grow above the dotted line at the two data points with the highest energies. This is likely due to spurious contributions from ICFα events, which, according to PACE estimates, become relevant at the highest energies of the experiment.

In the calculation of the CFFs of Figs. 10(a)–10(d), we used the radii of the Coulomb barriers of the SPP and the approximate expression for $f_{\mathrm{R}}(y)$ [Eq. (54)]. The barrier parameters of the SPP for the weakly bound systems studied in the present work are listed in Table III.

Now we introduce another method to investigate the suppression of CF in collisions of weakly bound projectiles. It consists in evaluating the ratio of the experimental cross sections to the fusion cross section of the BPM, which can be replaced by the cross section $\overline{\sigma}_{\mathrm{W}}$, to a very good approximation (see Fig. 5). That is,

$$\overline{\mathcal{H}}(y) = \frac{\sigma_{\mathrm{F}}^{\mathrm{expt}}(y)}{\overline{\sigma}_{\mathrm{W}}(y)}. \tag{67}$$

It is then plotted as a function of the reduced energy variable y. Similar procedures have already been used by other authors to measure the suppression of CF in collisions of weakly bound projectiles (see, e.g., Refs. [47,61,62]).

We used the ratio of Eq. (67) to investigate the suppression of CF in collisions of ^{6}Li with the same targets as Fig. 10(a). The results are shown in Fig. 11(b). For comparison, Fig. 11(a) shows a similar figure for the tightly bound systems of Fig. 9. At above-barrier energies, the experimental points for tightly bound systems are close to one (the dashed line), whereas those for ^{6}Li projectiles fall well below, around 0.6 (dotted line). Thus, the function $\overline{\mathcal{H}}(y)$ can be used to investigate the suppression of CF above the Coulomb barrier. However, this ratio systematically increases as y decreases toward the Coulomb barrier and below it, both for weakly and tightly bound systems. The reason is that, in this energy region, this ratio is very sensitive to the exact value of the Coulomb barrier and any channel coupling effect, even very weak ones. Thus, associating this behavior with any particular static or dynamic property of the colliding system may be misleading.

To close this section, we emphasize that the reduction methods discussed in this section lead to universal functions that play the role of a benchmark to which reduced fusion data should be compared. Since the influence of trivial factors like the charges and sizes of the collision partners are washed out

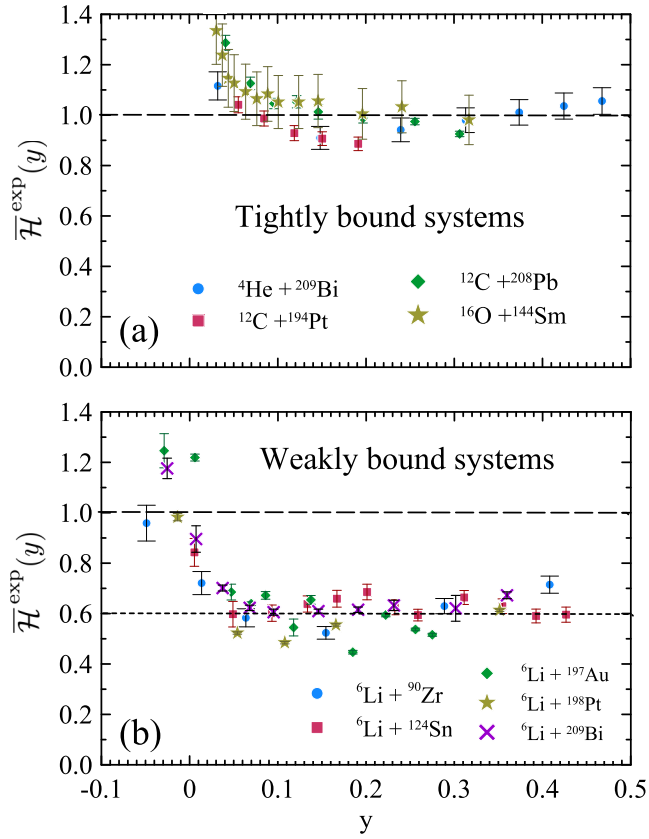

FIG. 11. The ratio $\overline{\mathcal{H}}(y)$ for (a) tightly bound and (b) weakly bound systems.

by the reduction procedure, deviations from the benchmark indicate the influence of nuclear structure effects. However, it has been assumed that the reduction is carried out with parameters of a potential that describes experimental fusion cross sections in the absence of nuclear structure effects. If the barrier parameters are determined by fitting fusion data, the reduced cross section will also account for the effects of the nuclear structure that one wants to investigate. In this way, it tends to reproduce the universal function of the model, and no useful information can be extracted from the comparison.

VI. CONCLUSIONS

We derived an improved version of the Wong formula for heavy-ion fusion that is valid under conditions where the standard Wong formula is inaccurate. This is achieved by replacing the *s*-wave barrier parameters in the Wong formula with the parameters of the *l*-dependent potential barrier at an effective partial wave, given by an average over angular momentum. The same procedure is used to obtain an improved expression for the classical fusion cross section.

The improved Wong cross sections for systems over a broad mass range were compared with the corresponding cross sections of the barrier penetration model. They were shown to be in excellent agreement. An analogous comparison was made for the improved classical fusion cross sections of the same systems. In this case, it was restricted to energies above the Coulomb barrier. The agreement with the barrier penetration model cross section was also extremely good.

Based on the improved classical cross sections, we proposed a new procedure to reduce the fusion data of different systems. This procedure, which we call the *classical fusion function* method, leads to a new universal function, the *classical fusion line*, which plays the role of a benchmark in comparisons of reduced fusion data. This method was used to study the suppression of complete fusion in collisions of weakly bound projectiles. Comparisons of reduced cross sections in collisions of ^{6}Li and ^{7}Li with targets over a wide mass range lead to two conclusions: (*i*) The suppression increases as the breakup threshold of the projectile increases, (*ii*) the suppression does not seem to depend on the target charge. This indicates that the suppression of complete fusion is mainly due to nuclear breakup couplings.

ACKNOWLEDGMENTS

Work was supported in part by the Brazilian funding agencies, CNPq, FAPERJ, CAPES, and the INCT-FNA (Instituto Nacional de Ciência e Tecnologia- Física Nuclear e Aplicações), research project 464898/2014-5, and the Uruguayan agencies PEDECIBA (Programa de Desarrollo de las Ciencias Básicas) and ANII (Agencia Nacional de Innovación e Investigación). We are indebted to Dr. Roberto Linares for critically reading the manuscript.

[1] L. F. Canto, P. R. S. Gomes, R. Donangelo, and M. S. Hussein, Phys. Rep. **424**, 1 (2006).
[2] N. Keeley, R. Raabe, N. Alamanos, and J. L. Sida, Prog. Part. Nucl. Phys. **59**, 579 (2007).
[3] N. Keeley, N. Alamanos, K. W. Kemper, and K. Rusek, Prog. Part. Nucl. Phys. **63**, 396 (2009).
[4] L. F. Canto, P. R. S. Gomes, R. Donangelo, J. Lubian, and M. S. Hussein, Phys. Rep. **596**, 1 (2015).
[5] J. J. Kolata, V. Guimarães, and E. F. Aguilera, Eur. Phys. J. A **52**, 123 (2016).
[6] L. Canto, V. Guimarães, J. Lubian, and M. Hussein, Eur. Phys. J. A **56**, 281 (2020).
[7] L. C. Chamon, D. Pereira, M. S. Hussein, M. A. Candido Ribeiro, and D. Galetti, Phys. Rev. Lett. **79**, 5218 (1997).
[8] L. C. Chamon, B. V. Carlson, L. R. Gasques, D. Pereira, C. De Conti, M. A. G. Alvarez, M. S. Hussein, M. A. Cândido Ribeiro, E. S. Rossi Jr., and C. P. Silva, Phys. Rev. C **66**, 014610 (2002).
[9] R. O. Akyüz and A. Winther, in *Nuclear Structure of Heavy Ion Reaction*, edited by R. A. Broglia, C. H. Dasso, and R. A. Ricci (North Holland, Amsterdam, 1981).
[10] C. Y. Wong, Phys. Rev. Lett. **31**, 766 (1973).
[11] L. F. Canto, D. R. Mendes Junior, P. R. S. Gomes, and J. Lubian, Phys. Rev. C **92**, 014626 (2015).
[12] L. F. Canto, P. R. S. Gomes, J. Lubian, L. C. Chamon, and E. Crema, J. Phys. G **36**, 015109 (2009).
[13] L. F. Canto, P. R. S. Gomes, J. Lubian, L. C. Chamon, and E. Crema, Nucl. Phys. A **821**, 51 (2009).
[14] L. F. Canto, P. R. S. Gomes, J. Lubian, P. Lotti, L. C. Chamon, and E. Crema, Phys. Rev. C **80**, 034615 (2009).
[15] L. R. Gasques, L. C. Chamon, P. R. S. Gomes, and J. Lubian, Nucl. Phys. A **764**, 135 (2006).

[16] G. H. Rawitscher, Nucl. Phys. **85**, 337 (1966).
[17] K. Hagino, N. Rowley, and A. T. Kruppa, Comput. Phys. Commun. **123**, 143 (1999).
[18] E. C. Kemble, Phys. Rev. **48**, 549 (1935).
[19] D. L. Hill and J. A. Wheeler, Phys. Rev. **89**, 1102 (1953).
[20] A. J. Toubiana, L. F. Canto, and M. S. Hussein, Eur. Phys. J. A **53**, 34 (2017).
[21] N. Rowley and K. Hagino, Phys. Rev. C **91**, 044617 (2015).
[22] C. Y. Wong, Phys. Rev. C **86**, 064603 (2012).
[23] L. F. Canto, P. R. S. Gomes, J. Lubian, M. S. Hussein, and P. Lotti, Eur. Phys. J. A **50**, 89 (2014).
[24] M. S. Hussein, P. R. S. Gomes, J. Lubian, and L. C. Chamon, Phys. Rev. C **73**, 044610 (2006).
[25] M. R. Cortes, J. Rangel, J. L. Ferreira, J. Lubian, and L. F. Canto, Phys. Rev. C **102**, 064628 (2020).
[26] J. Lubian, J. L. Ferreira, J. Rangel, M. R. Cortes, and L. F. Canto, Phys. Rev. C **105**, 054601 (2022).
[27] J. L. Ferreira, J. Rangel, J. Lubian, and L. F. Canto, Phys. Rev. C **107**, 034603 (2023).
[28] M. Cavallaro, F. Cappuzzello, M. Bondì, D. Carbone, V. N. Garcia, A. Gargano, S. M. Lenzi, J. Lubian, C. Agodi, F. Azaiez *et al.*, Phys. Rev. C **88**, 054601 (2013).
[29] A. Spatafora, D. Carbone, F. Cappuzzello, M. Cavallaro, L. Acosta, C. Agodi, P. Amador-Valenzuela, T. Borello-Lewin, G. A. Brischetto, S. Calabrese *et al.* (NUMEN Collaboration), Phys. Rev. C **107**, 024605 (2023).
[30] F. Cappuzzello, H. Lenske, M. Cavallaro, C. Agodi, N. Auerbach, J. Bellone, R. Bijker, S. Burrello, S. Calabrese, D. Carbone *et al.*, Prog. Part. Nucl. Phys. **128**, 103999 (2023).
[31] R. A. Broglia and A. Winther, *Heavy Ion Reactions* (Westview Press, Cambridge, 2004).
[32] P. R. S. Gomes, J. Lubian, and L. F. Canto, Phys. Rev. C **79**, 027606 (2009).
[33] P. R. S. Gomes, L. F. Canto, J. Lubian, and M. S. Hussein, Phys. Lett. B **695**, 320 (2011).
[34] B. Wang, W. J. Zhao, P. R. S. Gomes, E. G. Zhao, and S. G. Zhou, Phys. Rev. C **90**, 034612 (2014).
[35] F. Gollan, D. Abriola, A. Arazi, M. A. Cardona, E. de Barbará, J. de Jesús, D. Hojman, R. M. Id. Betan, J. Lubian, A. J. Pacheco, B. Paes, D. Schneider, and H. O. Soler, Phys. Rev. C **104**, 024609 (2021).
[36] J.-M. Yang, Z.-W. Song, W.-J. Zhao, and B. Wang, Phys. Rev. C **104**, 034607 (2021).
[37] I. M. Bhat, M. Shuaib, M. S. Asnain, V. R. Sharma, A. Yadav, M. K. Sharma, P. P. Singh, D. P. Singh, U. Gupta, R. N. Sahoo *et al.*, Nucl. Phys. A **1021**, 122421 (2022).
[38] A. A. Hassan, S. M. Luk'yanov, R. Kalpakchieva, Y. E. Penionzhkevich, R. A. Astabatyan, I. Vinsour, A. A. Dlouhy, Z. Kulko, J. Mrazek, S. P. Lobastov, E. R. Markaryan *et al.*, Izv. Rossiiskoi Akademii Nauk **70**, 1558 (2006).
[39] A. Shrivastava, S. Kailas, A. Chatterjee, A. Navin, A. M. Samant, P. Singh, S. Santra, K. Mahata, B. S. Tomar, and G. Pollarolo, Phys. Rev. C **63**, 054602 (2001).
[40] A. Mukherjee, D. J. Hinde, M. Dasgupta, K. Hagino, J. O. Newton, and R. D. Butt, Phys. Rev. C **75**, 044608 (2007).
[41] J. R. Leigh, M. Dasgupta, D. J. Hinde, J. C. Mein, C. R. Morton, R. C. Lemmon, J. P. Lestone, J. O. Newton, H. Timmer, J. X. Wei, and N. Rowley, Phys. Rev. C **52**, 3151 (1995).
[42] M. Dasgupta, D. J. Hinde, K. Hagino, S. B. Moraes, P. R. S. Gomes, R. M. Anjos, R. D. Butt, A. C. Berriman, N. Carlin, C. R. Morton *et al.*, Phys. Rev. C **66**, 041602(R) (2002).
[43] M. Dasgupta, P. R. S. Gomes, D. J. Hinde, S. B. Moraes, R. M. Anjos, A. C. Berriman, R. D. Butt, N. Carlin, J. Lubian, C. R. Morton *et al.*, Phys. Rev. C **70**, 024606 (2004).
[44] A. Shrivastava, A. Navin, A. Lemasson, K. Ramachandran, V. Nanal, M. Rejmund, K. Hagino, T. Ishikawa, S. Bhattacharyya, A. Chatterjee, and S. Kailas, K. Mahata, V. V. Parkar, R. G. Pillay, and P. C. Rout, Phys. Rev. Lett. **103**, 232702 (2009).
[45] C. S. Palshetkar, S. Thakur, V. Nanal, A. Shrivastava, N. Dokania, V. Singh, V. V. Parkar, P. C. Rout, R. Palit, R. G. Pillay, S. Bhattacharyya, A. Chatterjee, S. Santra, K. Ramachandran, and N. L. Singh, Phys. Rev. C **89**, 024607 (2014).
[46] V. V. Parkar, S. K. Pandit, A. Shrivastava, R. Palit, K. Mahata, V. Jha, K. Ramachandran, S. Gupta, S. Santra, S. K. Sharma *et al.*, Phys. Rev. C **98**, 014601 (2018).
[47] H. Kumawat, V. Jha, V. V. Parkar, B. J. Roy, S. K. Pandit, R. Palit, P. K. Rath, C. S. Palshetkar, S. K. Sharma, S. Thakur, A. K. Mohanty, A. Chatterjee, and S. Kailas, Phys. Rev. C **86**, 024607 (2012).
[48] A. Shrivastava, A. Navin, A. Diaz-Torres, V. Nanal, K. Ramachandran, M. Rejmund, S. Bhattacharyya, A. Chatterjee, S. Kailas, A. Lemasson *et al.*, Phys. Lett. B **718**, 931 (2013).
[49] National Nuclear Data Center-NNDC, Brookhaven National Laboratory (2018), http://www.nndc.bnl.gov/.
[50] F. M. Nunes and I. J. Thompson, Phys. Rev. C **57**, R2818 (1998).
[51] F. M. Nunes and I. J. Thompson, Phys. Rev. C **59**, 2652 (1999).
[52] D. R. Otomar, P. R. S. Gomes, J. Lubian, L. F. Canto, and M. S. Hussein, Phys. Rev. C **87**, 014615 (2013).
[53] P. Descouvemont, L. F. Canto, and M. S. Hussein, Phys. Rev. C **95**, 014604 (2017).
[54] P. R. S. Gomes, J. Lubian, B. Paes, V. N. Garcia, D. S. Monteiro, I. Padrón, J. M. Figueira, A. Arazi, O. A. Capurro, L. Fimiani *et al.*, Nucl. Phys. A **828**, 233 (2009).
[55] G. S. Li, J. G. Wang, J. Lubian, H. O. Soler, Y. D. Fang, M. L. Liu, N. T. Zhang, X. H. Zhou, Y. H. Zhang, B. S. Gao *et al.*, Phys. Rev. C **100**, 054601 (2019).
[56] M. Kaushik, G. Gupta, S. Thakur, H. Krishnamoorthy, P. P. Singh, V. V. Parkar, V. Nanal, A. Shrivastava, R. G. Pillay, K. Mahata *et al.*, Phys. Rev. C **101**, 034611 (2020).
[57] Y. D. Fang, P. R. S. Gomes, J. Lubian, X. H. Zhou, Y. H. Zhang, J. L. Han, M. L. Liu, Y. Zheng, S. Guo, J. G. Wang *et al.*, Phys. Rev. C **87**, 024604 (2013).
[58] J. J. Kolata, V. Guimarães, D. Peterson, P. Santi, R. White-Stevens, P. A. De Young, G. F. Peaslee, B. Hughey, B. Atalla, M. Kern *et al.*, Phys. Rev. Lett. **81**, 4580 (1998).
[59] J. J. Kolata, V. Guimarães, D. Peterson, P. Santi, R. White-Stevens, J. von Schwarzenberg, J. D. Hinnefeld, E. F. Aguilera, E. Martinez-Quiroz, D. A. Roberts *et al.*, Phys. Rev. C **57**, R6(R) (1998).
[60] R. Raabe, J. L. Sida, J. L. Chavet, N. Alamanos, C. Angulo, J. M. Casandjian, S. Courtin, A. Drouart, C. Durand, P. Figuera *et al.*, Nature (London) **431**, 823 (2004).
[61] V. V. Parkar, R. Palit, S. K. Sharma, B. S. Naidu, S. Santra, P. K. Joshi, P. K. Rath, K. Mahata, K. Ramachandran, T. Trivedi *et al.*, Phys. Rev. C **82**, 054601 (2010).
[62] L. R. Gasques, D. J. Hinde, M. Dasgupta, A. Mukherjee, and R. G. Thomas, Phys. Rev. C **79**, 034605 (2009).